Colloidal Titanium Nitride Nanobars for Broadband Inexpensive Plasmonics and Photochemistry from Visible to Mid-IR Wavelengths

Colloidal Titanium Nitride Nanobars for Broadband Inexpensive Plasmonics and Photochemistry from Visible to Mid-IR Wavelengths

Sourav Rej,[a] Eva Yazmin Santiago,[b] Olga Baturina,[c] Yu Zhang,[a] Sven Burger,[d] Štěpán Kment,[a,e] Alexander O. Govorov*[,b] and Alberto Naldoni*[,a,f]

[a]Dr. S. Rej, Dr. Y. Zhang, Dr. S. Kment, Prof. A. Naldoni

Czech Advanced Technology and Research Institute, Regional Centre of Advanced Technologies and Materials Department, Palacký University Olomouc. Šlechtitelů 27, 78371 Olomouc, Czech Republic.

[b]E. Y. Santiago, Prof. A. O. Govorov

Department of Physics and Astronomy, Nanoscale and Quantum Phenomena Institute, Ohio University Athens, Ohio 45701, United States.

[c]Dr. O. Baturina

Chemistry Division, United States Naval Research Laboratory, Washington, D.C. 20375, United States.

[d]Dr. S. Burger

Zuse Institute Berlin, 14195 Berlin, Germany, JCMwave GmbH, 14050 Berlin, Germany.

[e]Dr. S. Kment

CEET, Nanotechnology Centre, VŠB-Technical University of Ostrava, 17. Listopadu 2172/15, 708 00, Ostrava-Poruba, Czech Republic.

[f]Prof. A. Naldoni

Department of Chemistry and NIS Centre, University of Turin, 10125 Turin, Italy.

[*]Corresponding authors. E-mail address: alberto.naldoni@unito.it (A. Naldoni), govorov@ohio.edu (A. O. Govorov)

Abstract

Developing colloidal plasmonic nanomaterials with high carrier density that show optical resonances and photochemical activity extending from the visible to the mid-infrared (MIR) ranges remains a challenging pursuit. Here, we report the fabrication of titanium nitride (TiN) nanobars obtained using a two–step procedure based on a wet chemical route synthesis of TiO_2 nanowires and their subsequent high temperature annealing in ammonia flow. Electromagnetic simulations of the resulting TiN nanobars reveal a rich set of optical resonances featuring transverse, longitudinal and mixed transverse–longitudinal plasmonic modes that cover energies from the visible to MIR region. TiN nanobars decorated with Pt co-catalyst nanocrystals show enhanced photocatalytic hydrogen evolution activity in comparison to both isotropic TiN nanospheres of similar size and TiN nanocubes under near infrared excitation at 940 nm due to the enhanced hot electron generation. We also demonstrate that plasmonic TiN nanobars can be used for the detection of furfural molecular vibrations by providing a strong surface enhanced infrared absorption (SEIRA) effect in the MIR region.

Keywords

NIR plasmonic, titanium nitride, hydrogen evolution, photo thermal, SEIRA sensing

1. Introduction

In modern nanotechnology, plasmonics provides probably the finest control over light-matter interactions using metallic nanostructures supporting in–phase oscillations of conducting electrons strongly coupled to and excited by incoming photons. A relevant property of plasmonic nanostructures is their ability to concentrate light (and electromagnetic near fields) in nanoscale volumes, enabling strong enhancement of many physical and chemical phenomena underlying non–linear optics [1], sensing [2], heat transfer [3,4], and chemical reactions [5–7] among others. Once the plasmonic excitation decays, the stored energy can be transferred to adjacent objects (solid materials, molecules, fluids) either through plasmonic non–thermal (hot) carriers or by the significant lattice heating reached after their thermalization [5,8]. A flurry of promising experiments leveraging plasmonic effects have demonstrated that plasmonics will have a transformative impact on the energy technologies of the future [9]. Notably, the excitation wavelength of localized surface plasmon resonances (LSPRs) in plasmonic nanostructures defines their operational energy range (and therefore their application) and depend on the carrier density of the employed material, on the shape/size of the nanoresonator, and on its dielectric environment. For instance, plasmonic photocatalysts working in the visible region of the electromagnetic spectrum usually employ Au, Ag, Al, and TiN. The latter shows gold–like optical properties in the visible region [10], while presenting high chemical stability in harsh environments (i.e. strong acids), high hardness, and extreme resistance to temperature (being a refractory metal) that make TiN an outstanding candidate material for several energy applications [11–13].

Apart from anisotropic Au nanocrystals like rods, plates and bipyramids[14,15] LSPR absorption in the near infrared (NIR) region can also be achieved by introducing element vacancy in semiconductors such as copper chalcogenides ($Cu_{2-x}S$, Cu_7S_4) [16–18], tungsten oxides (WO_{3-x}, $W_{18}O_{49}$) [19–22], MoO_{3-x} [23], and Bi_2O_{3-x} [24] which have shown photocatalytic activity in the NIR region. In addition, colloidal degenerate indium nitride (InN) nanocrystals showed an LSPR absorption reaching the mid-IR (~3000 nm) region [25]. The mid–IR wavelength range is relevant for health- and defense-related applications including trace-gas detection, heat-signature sensing, thermal auditing, mimicking and cloaking, and source and detector development [26]. More importantly for energy applications, plasmonic devices working the mid–IR range find use in chemical sensing (or to track reaction products), as the majority of molecular vibrations fall in this energy range and can be amplified by the plasmonic near fields through the surface enhanced IR absorption (SEIRA) effect [2]. However, suitable materials for the mid-IR range are usually obtained by

designing metasurfaces using complex nanoantenna geometries and expensive fabrication methods [27,28]. It is indeed challenging to achieve colloidal plasmonic nanostructures with LSPR resonances in the mid–IR using metals with high carrier density.

To address this major limitation, here we report the synthesis of photochemically active plasmonic TiN nanobars showing a multitude of resonances extending from the visible to the mid-IR region. Full-wave electromagnetic simulations reveals in details the superior optical properties of these anisotropic nanostructures in comparison to isotropic nanoparticles of comparable size. We validate the use of the investigated plasmonic TiN colloids, by testing them in plasmon–enhanced hydrogen evolution under monochromatic NIR light irradiation at 940 nm and comparing the shape-dependent photocatalytic activity of Pt-loaded nanocubes, nanospheres and nanobars, demonstrating the action of a hot electron driven mechanism. Moreover, we show that plasmonic TiN nanobars can be employed to detect energy-relevant molecules such as furfural by providing a strong SEIRA effect.

2. Results and Discussion

The studied plasmonic TiN nanostructures were prepared starting from the hydrothermal synthesis of the precursor TiO_2 nanomaterials adopting modified reported methods [29,30]. In one case, we obtained first hydrogen titanate ($H_2Ti_3O_7$) nanowires, which were converted into TiO_2 nanowires upon calcination at 400 °C for 1 h (Fig. 1a and S1). In the second case, we prepared TiO_2 nanospheres composed by the assembly of TiO_2 nanosheets (Fig. S2). Next, TiN nanobars and nanospheres were achieved by conversion of the TiO_2 nanostructures via nitridation at 800 °C for 5 h (see *Methods* in Supporting Information). A complete structural and morphological characterization of TiO_2 and TiN nanostructures confirmed the complete conversion to titanium nitride in both cases (Fig. 1b, 1c and S3–S9). TiN nanobars show an average length, width and height of 1200, 220 and 40 nm, respectively (Fig. 1d and S5), featuring nanosized holes on their surface (Fig. 1e–k). In contrast, TiN nanospheres show an average diameter of 200 nm and consist of complex spherical superstructures featuring surface nanoridges (Fig. S3). TiN nanobars present higher specific surface area (55.9 $m^2 g^{-1}$) than the TiN nanospheres (46.8 $m^2 g^{-1}$) (Fig. S10). Formation of nanoholes on the surface of TiN nanostructures is due to the high temperature anion exchange and phase transition process, which can be explained recalling the Kirkendall mechanism in the presence of hot ammonia (Fig. S7). The dark field scanning TEM image and energy-dispersive X-ray spectroscopy (EDS) elemental mapping (Fig. 1f–k) of TiN nanobars homogenously decorated with Pt nanocrystals (functional for the photocatalytic experiments shown below, for further characterizations see also Fig. S11–S13) provided nanoscale details

on the nanoholes present on their surface. Fig. 1i shows the presence of oxygen in the elemental mapping due to the presence of an ultrathin amorphous oxide layer composed of titanium oxynitride (TiON) and titanium oxide (TiO_2) on the surface of TiN nanobars, as evidenced by HRTEM (Fig. S14) and XPS (Fig. S15, S16 and Table S1). The native oxide layer is commonly formed on TiN nanostructures upon exposure to air and/or water during chemical processing [31].

The UV–vis–NIR absorption spectra measured in dichloromethane show that for both the TiO_2 nanostructures the absorption is mainly limited to the UV region (Fig. 2a and S17), with a characteristic tail in the visible region due to the light scattering produced by the nanostructures in suspension. In contrast, both the TiN nanomaterials present the characteristic interband transitions feature up to ~500 nm [31], after which a broad and intense plasmon peak rises reaching the maximum in the NIR region. Interestingly, after 1300 nm, the absorption spectrum of TiN nanospheres decline, whereas for the nanobars, it kept the same intensity even beyond 2200 nm. To retrieve absorption data in a wider energy range, we measured attenuated total reflection-Fourier transform infrared (ATR-FTIR) spectra of the plasmonic TiN nanostructures (Fig. 2b and Fig. S18), showing that the absorption extends to the entire mid-IR wavelength range. We think that the observed broadband character of absorption is due to the size dispersion of TiN nanostructures and to their partial aggregation in colloidal suspension. This conclusion was confirmed by us using theoretical calculations.

To assess precisely the plasmonic properties of the TiN nanobars, we performed electromagnetic field propagation using finite-element software (COMSOL and JCMsuite). Geometrical features were retrieved from TEM micrographs (for width and length, see Fig. S5) and AFM height profile (for thickness, Fig. 1d). The width (220 nm) and thickness (40 nm) of the nanobars were kept constant, while the length was the sweeping parameter (200, 400, 800, 1200 nm). To account for the random orientation of the plasmonic nanobars in solution, the calculated spectra were averaged over three orthogonal propagation directions of light and two polarizations, thus leading to spectra featuring transverse (T), longitudinal (L) and mixed transverse–longitudinal (T–L) plasmonic modes (Fig. 2c and Fig. S20–S24). When we considered even more incident light directions (12 to 60) the observation of an additional plasmonic peak at ~2500 nm was possible (Fig. S25). To account for the granular structure featured in the nanobars (Fig. 1b), we implemented the simulations by using a homogeneous dielectric function derived within the effective medium theory, where the TiN and dichloromethane volume fractions were 0.7 and 0.3, respectively. More details on the calculations can be found in the Supporting Information. Notably, the adoption of an

effective medium dielectric function resulted in predicting relevant differences in the optical properties of the TiN nanobars as compared to the case where a metallic dielectric constant was used (Fig. S26). In particular, for the case of hybrid TiN nanobars with 1200 nm length, we observed two main effects: (i) a red shift of the plasmonic peaks, and (ii) an increased absorption fraction over scattering, especially at mid–IR wavelengths. Fig. 2c shows the averaged mass extinction coefficient (MEC) of the TiN nanobars with different lengths. This parameter quantifies how easily light is extinguished by the volume (mass) of the material, and it was calculated by dividing the optical cross sections with the mass of the nanostructure (see Supporting Information).

Increasing the anisotropy of the nanostructure, i.e. length ≥ 400 nm, three clear kinds of plasmonic resonances appear in the spectra. The surface charge maps at peak wavelengths obtained for specific light propagation direction (and polarization) provides insights into the nature of those plasmonic resonance breeds, denoted here as L, T1, and T2 (Fig. 2d–i and S24). The intense peak in the visible region (642 nm for length=1200 nm) is due to the mixed T_2–T_1 transverse plasmonic mode and appears at similar wavelengths for nanobars with different lengths. A similar behavior is followed by the strong extinction peak in the NIR region (1262 nm for length=1200 nm), which is due to the mixed T_1–L plasmonic mode. In contrast, the most intense peak is assigned to the purely L plasmonic resonance and its position can be tuned from 2154 to 5266 nm by varying the TiN nanobar length from 400 to 1200 nm, respectively. Interestingly, the plasmonic peaks show increased bandwidth at longer wavelengths, reaching 1000–3000 nm full widths at half maximum for the mid–IR resonance. The computed spectral structure of plasmonic resonances is amazingly rich, and each spectral feature on the computed spectrum can be assigned to a certain resonance of this TiN plasmonic “flute”. In addition, we found that the absorption and scattering efficiencies of the TiN nanobars are, in general, comparable (Fig. 2j and 2k). We note that the absorption efficiency is the most relevant parameter for the photochemical conversion, since it directly describes the portion of the photon energy, which become absorbed, i.e., get converted into heat and hot electrons. Simulated optical properties and related discussion for TiN nanospheres in detail can be found in the Supporting Information (Fig. S27–S30).

Notably, these results highlight the possibility to design TiN plasmonic nanostructures with high anisotropy suitable for plasmonic applications in a wide range of operational energies starting from the UV and extending to the mid-IR (300 nm – 6 μm).

To demonstrate the potential of plasmonic TiN nanobars, we tested their application both in plasmonic photocatalysis in NIR region and in SEIRA in the mid–IR energy range. Firstly, we selected plasmon–enhanced H_2 evolution through dehydrogenation of ammonia borane as a model reaction to compare the photocatalytic activity of TiN nanobars with nanospheres and nanocubes using monochromatic NIR excitation at 940 nm. Detailed calculation about photothermal turnover frequency (TOF_{photo}), thermal turnover frequency (TOF_{therm}), and hot electron turnover frequency ($TOF_{hot–e}$) can be found in the Supporting Information. We recently showed that TiN nanocubes can efficiently drive this reaction under both solar irradiation and monochromatic visible light, upon functionalization with Pt nanocrystals. The generation of plasmonic hot electrons was mainly localized in the TiN nanostructure (followed by their injection into the Pt component), while a smaller fraction of hot carriers was directly generated in the Pt nanocrystals [31]. Consequently, we functionalized the prepared TiN nanostructures with homogeneously dispersed Pt nanocrystals with an average diameter of 2.6 nm (Fig. S11, S12 and S31). As a result, we obtained TiN/Pt nanohybrids where the TiN component dominates the plasmonic properties, whereby Pt is the catalytic centre. The pure TiN nanostructures did not produce any considerable H_2 amount both under dark and light conditions. In contrast, we detected rapid H_2 evolution when TiN/Pt nanohybrids were employed as the photocatalysts (Fig. S32 and S33). The enhanced activity observed under light irradiation is attributed to plasmonic effects. The Pt nanocrystals themselves did not show any significant contribution as a photocatalyst during the light-assisted H_2 evolution, as confirmed by the identical reaction kinetics under dark and light conditions obtained by using Pt nanocrystals supported on an optically inactive Al_2O_3 support (Fig. S34). Even anatase TiO_2/Pt nanowires did not show any photoactivity under 940 nm NIR light illumination, suggesting that the ultrathin TiO_2 layer on TiN nanobars had no contribution in the overall hydrogen production rate (Fig. S35). To determine the advantage of using the anisotropic TiN/Pt nanobars resonators in plasmonic catalysis, we compared their activity with Pt loaded TiN nanospheres and nanocubes. Using light excitation at 940 nm at a power density of 24 mW cm^{-2}, we measured $TOF_{hot\text{-}e}$ for different TiN shapes (Fig. 3a) in the experimental regime under constant temperature, i.e., when the low intensity light irradiation did not produce any significant macroscopic variation (and microscopic, see below and Supporting Information) [31–33] of the solution temperature. In this case, we avoid the thermal chemical mechanism and deal only with hot electrons. Notably, using the same Pt loading, TiN nanobars showed 1.67 and 2.41 times

higher plasmon–enhanced H_2 evolution activity than that showed by TiN nanospheres and nanocubes respectively (Fig. 3a, S32, S33 and Table S6). The performance of TiN nanobars can be further highlighted by calculating the apparent quantum yield (for details see Supporting Information), which was 120%, 71% and 49% for TiN nanobars, nanospheres, and nanocubes respectively. TiN/Pt nanobars show also excellent NIR photocatalytic activity if compared with reported noble metal photocatalysts like $Ag/W_{18}O_{49}$ nanowires (AQY_{1250nm} = 4%, see Table S7). To the best of our knowledge, this study provides first shape dependent plasmonic activity evaluation for TiN nanocrystals beyond 900 nm. Such unique NIR activity of TiN nanobars makes it suitable candidate for maximum utilization of solar light as well as under NIR (700−2500 nm) light. The TiN/Pt nanobars maintained their catalytic performance and structure even after three consecutive photocatalytic cycles (Fig. S36–S38, Table S5).

To investigate the reasons behind this observation, we computed the mass extinction coefficient for the absorption channel (MEC_{abs}) at 940 nm for TiN nanobars and TiN nanospheres with different sizes (Fig. 3b). TiN nanobars show generally higher MECs than TiN nanospheres, especially when the shape become more anisotropic (length ≥ 400 nm). Moreover, considering the optical cross sections at 940 nm (and the absorption/scattering efficiency reported in Fig. S30), TiN nanobars present similar values of both absorption and scattering cross sections, while for TiN nanospheres the scattering cross section is the double (or more for bigger sized nanospheres) the absorption one (Fig. S26 and S27). Hence, hot electron generation in nanobars can take place more efficiently due to the higher absorption fraction (i.e. less scattering), thereby resulting in higher TOF_{hot-e} value, which was calculated as $TOF_{hot-e} = TOF_{photo} - TOF_{thermo}$.

The efficiency of TiN/Pt nanobars were further examined under higher light intensities (producing appreciable heating) and at corresponding different final reaction temperatures (FT) in the dark (Fig. S39, Table S6). An in–depth kinetic study revealed a steady increase of TOF_{photo} with increasing light intensity (Fig. 3c). At 318 mW cm^{-2} power density, TOF_{photo} reached 242.3 $mol_{H2}\, mol_{Pt}^{-1} min^{-1}$ (see Table S7 for performance comparison with other photocatalysts reported in literature), with TiN/Pt nanobars showing a ~3.1-fold rate enhancement with respect to dark room temperature conditions because of the combined effect of both photothermal heating and hot electrons. Furthermore, the Supporting Information includes a list of FTs for different light intensities and for various TiN nanosystems (Table S6) and estimates of local temperature increase at the surface of a single nanostructure (Section: Theoretical modelling). As expected, the local temperature increase at

a nanoparticle is tiny, and the regime of photoheating in our study is collective, in which a large collective of nanocrystals contributes to the FT [31–33].

Interestingly, the difference between TOF_{therm} (Fig. 3c, blue bars) and TOF_{photo} (Fig. 3c, red bars) increased with increasing light intensity, suggesting a prominent hot electron effect at higher light intensity [7,31,34–36].

To confirm that a mechanism mediated by hot electrons is active even at high power density values, we computed Kinetic Isotope Effect (KIE) by comparing H_2 evolution rates obtained using D_2O and H_2O (Fig. S40 and 3d, see Supporting Information for more details on KIE calculation). The KIE value obtained in dark is 1.8, which confirms that the breaking of O−H bond in H_2O is the rate–determining step (RDS) during the ammonia borane dehydrogenation. KIE obtained under light illumination is 2.4, which is higher as compared to dark conditions, confirming that photocatalytic H_2 evolution is a hot electron-driven process [31,37].

The plasmonic effect on the activation energy (E_a) was also evaluated using the Arrhenius equation (Fig. 3e). Under dark, E_a was 36.6 kJ mol^{-1} (0.37 eV), while it decreased to 9.5 kJ mol^{-1} (0.09 eV) under 940 nm light irradiation. This confirms that plasmonic excitation of TiN/Pt nanobars produce hot electrons, which directly participate in the RDS of H_2 evolution reaction (i.e., O−H bond cleavage) and stabilizes the transition state (TS) by 0.28 eV (Fig. 3f and Fig. S41) [31]. Notably, this energy barrier reduction is higher than that one (0.1 eV, see Table S7) recently reported in a single-particle investigation study using Pt-tipped Au nanorods for the same chemical reaction. Moreover, we compare the energy barrier reduction for a selection of different reactions catalyzed by plasmonic photocatalysts recently appeared in the literature (Table S8). Despite some plasmonic photocatalysts provided impressive energy barrier reduction between 0.5 and 0.94 eV, most of them decreased the activation energy by 0.1−0.3 eV, similarly to the performance observed for TiN/Pt nanobars. This finding can also be extended to a non-noble metal co-catalyst systems. Interestingly, when we synthesised TiN/Ni nanobars, TiN nanobars were able to efficiently enhance plasmonic hydrogen production activity of Ni nanocrystals (Fig. S42) by the same factor observed for the activity of Pt nanocrystal under the same power density illumination at 940 nm. Thus, we have provided all the necessary figures of merit related to this plasmonic photocatalytic reaction [38].

Next, the TiN nanobars were tested in the mid-IR range for SEIRA enhancement by measuring spectral features of furfural, a relevant biomass derivative employed in chemical industry for the production of solvents, polymers fabrication, adhesives, pharmaceuticals, and

also a promising platform for photocatalytic H_2 production and biodiesel synthesis [39]. We compared the SEIRA enhancement obtained from TiN nanobars, Al_2O_3 (as inert substrate) and a common plasmonic material made by Au nanoparticles supported on Al_2O_3 (Fig. 4 and Fig. S43). For Al_2O_3 (blue line), the signal intensity is very low in the whole investigated energy range showing a clear peak only for the most intense furfural vibration at 1670 cm^{-1}, which is assigned to the aldehyde group stretching. When Au/Al_2O_3 (black line) used, the signal is slightly increased over the whole wavenumber range with many peaks arising and being more defined due to SEIRA effect produced by the plasmonic Au nanoparticles. In contrast, the spectrum measured using the plasmonic TiN nanobars substrate (red line) almost all the spectral features that can be also found in the reference spectrum of pure furfural (grey line). Notably, the SEIRA enhancements computed for all the detected peaks (Table S9) reach maximum values above 200 and span a vast energy range from 3000 to 13000 nm. These results are possible due to the broadband near fields generated in the plasmonic films made by aggregated TiN nanobars and that are shown to be superior that those generated in the reference sample containing Au nanoparticles [2].

To elaborate more on the SEIRA effect, we expect that with the SEIRA enhancement may correlate with the scattering efficiency of a nanobar. We now see from Fig. 2k that the scattering contribution, which also describes the induced dipole moment on a nanobar, is nearly constant over a wide range of nanorod sizes. Therefore, the nanobars of various sizes can be efficient for SEIRA. The other interesting observation from Fig. S26 is that the scattering strength and the field-enhancement should depend on the composition of our nanobars. For the effective-medium model, the scattering becomes weaker (almost twice) since the hybrid material is less plasmonic.

3. Conclusion

In summary, we fabricated plasmonic TiN nanobars through high temperature nitridation of TiO_2 nanowires showing a rich spectrum of electromagnetic resonances extending from the visible range to mid-IR range. We demonstrated the superior photocatalytic activity of TiN nanobars for hot electron driven photocatalytic hydrogen evolution providing the first shape-dependent plasmonic activity evaluation for TiN nanocrystals using NIR excitation, while also showing the applicability and significant SEIRA enhancements of furfural molecular vibrations in the mid-IR. These results open the way to the utilization of anisotropic plasmonic TiN nanostructures as plasmonic substrates for enhancing chemical reactions and the detection of reaction intermediates/products for energy–relevant processes. Importantly,

the developed colloidal nanostructures are made of an inexpensive, ceramic material, which is also highly thermally stable (refractory).

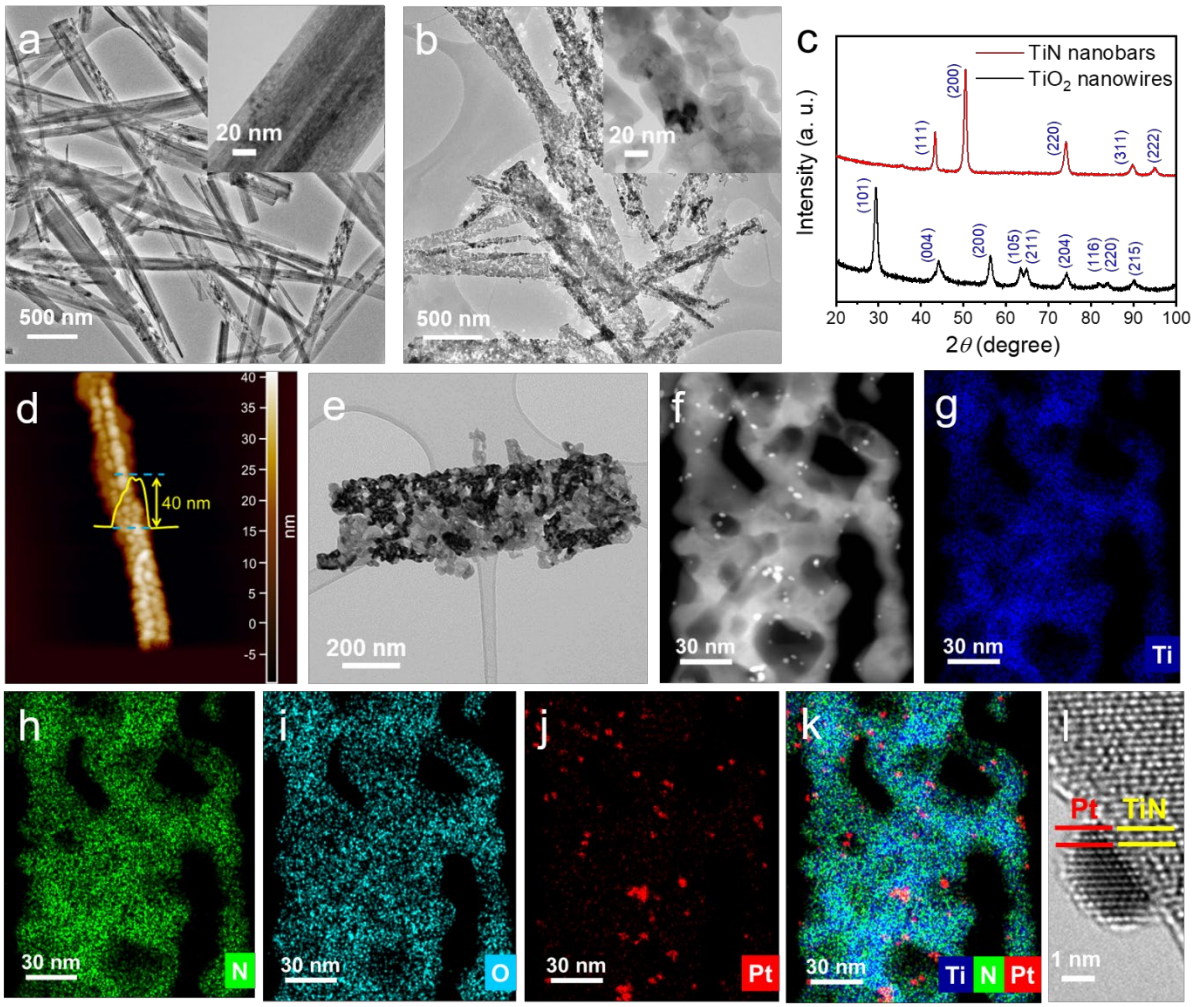

Fig. 1. Large area and magnified TEM images (inset) of (a) TiO_2 nanowires and (b) TiN nanobars. (c) X-ray diffraction patterns of TiO_2 nanowires and TiN nanobars. (d) AFM height profile of a single TiN nanobar. (e) Representative TEM image of a single TiN nanobar loaded with Pt nanoparticles. (f) HAADF–STEM image and (g–k) EDS elemental maps of a single TiN/Pt nanobar. (l) HRTEM micrograph of TiN/Pt nanobars showing the TiN/Pt sharp interface.

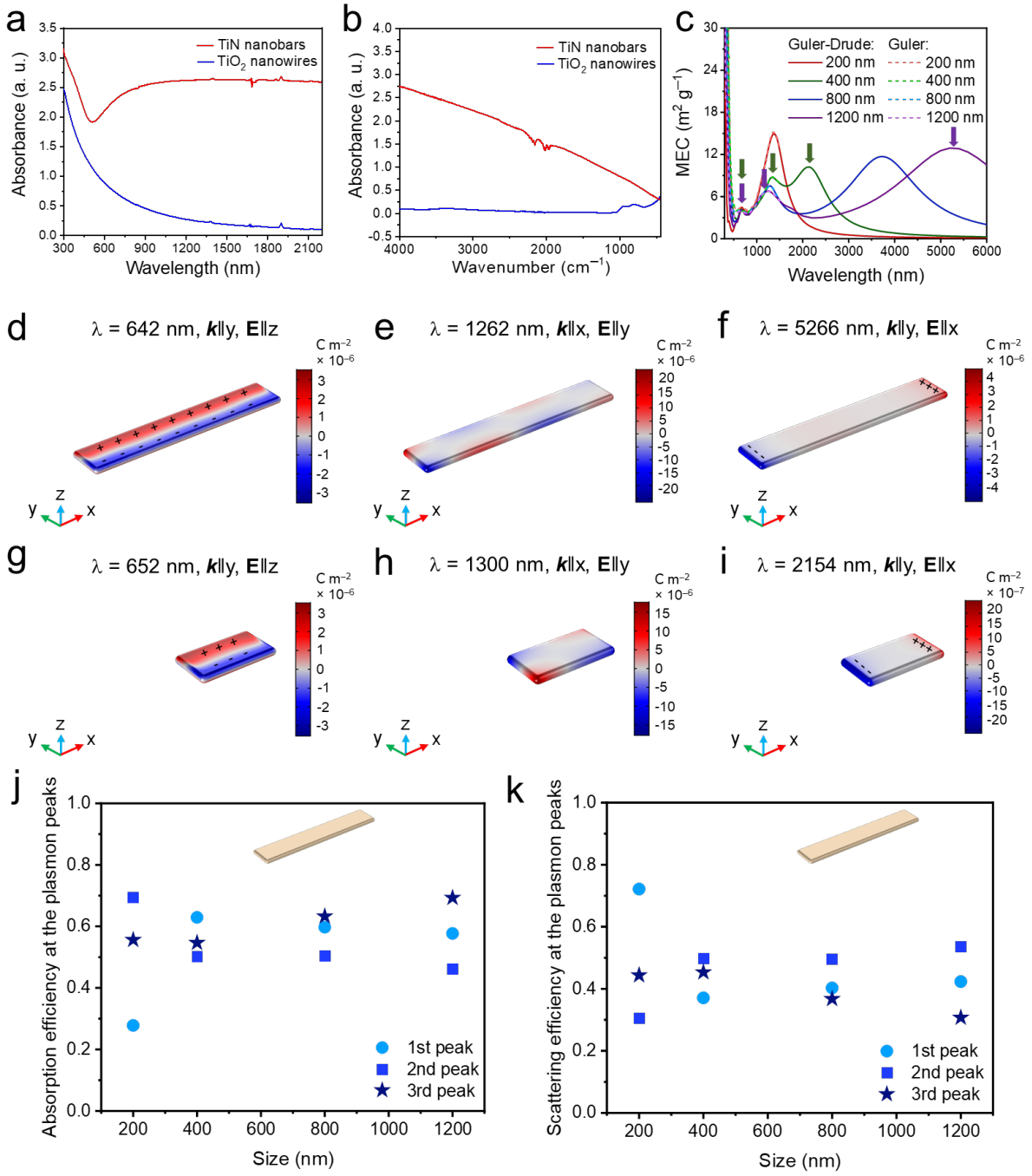

Fig. 2. (a) UV-vis-NIR absorption spectra of TiO_2 nanowires (blue line) and TiN nanobars (red line) in dichloromethane. (b) ATR-FTIR spectra of TiO_2 nanowires (blue line) and TiN nanobars (red line). (c) Comparison of Mass Extinction Coefficient (MEC) for different sizes of nanobars structures. Effective medium theory. Non-normalized averaged 6-direction. W= 0.22 μM, H = 0.04 μM, ε_m = TiN, ε_i = 2.02892, δ_i = 0.3. Simulated surface charge maps of plasmons for nanobars with two different lengths (d–f) 1200 nm, (g–i) 400 nm, keeping width and height fixed. (j,k) Absorption and scattering efficiencies of TiN nanobars with different lengths.

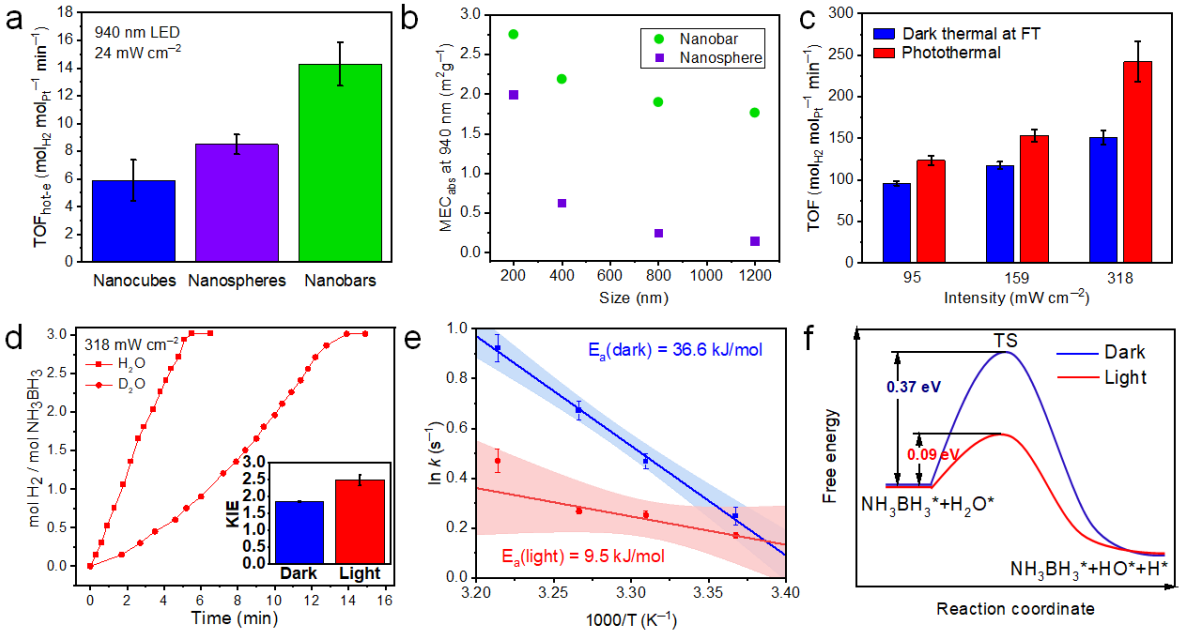

Fig. 3. (a) Plasmon–enhanced H_2 evolution rates expressed as hot electron–driven turnover frequency ($TOF_{hot\text{-}e}$) for the TiN/Pt nanohybrids with different shape in the constant-temperature experimental regime. (b) Absorption mass extinction coefficient (MEC_{abs}) at 940 nm for TiN nanobars (green circles) and TiN nanospheres (purple cubes) with different sizes. (c) TOF of H_2 evolution over TiN/Pt nanobars in dark at final temperature (FT) and under 940 nm excitation at different power density. (d) Kinetics of H_2 evolution with TiN/Pt nanobars in H_2O and D_2O. Inset shows Kinetic Isotope Effect (KIE) plot under dark and 940 nm light irradiation. (e) Arrhenius plots of apparent activation energies under light and dark conditions at FT showing coloured bands representing the 95% confidence interval of the linear fits. (f) Schematic representation of the free energy plots showing the energy barriers associated with the formation of the reaction transition state (TS) of the rate-determining step during NH_3BH_3 dehydrogenation under light and dark conditions. Asterisks denote species adsorbed on the catalyst surface. The error bar indicates the variation over three separate measurements.

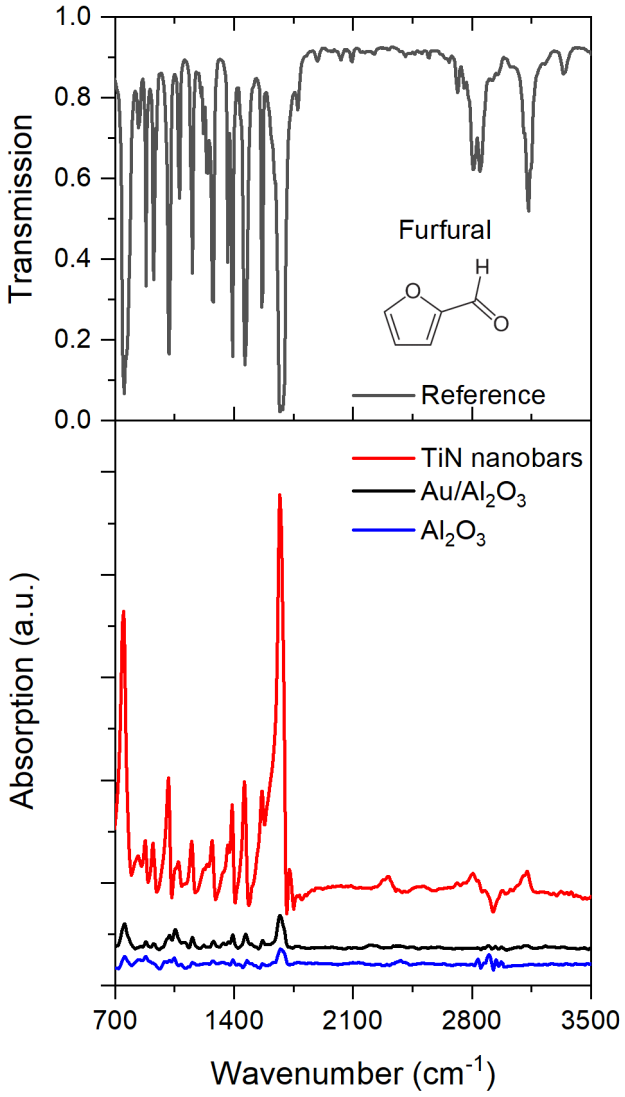

Fig. 4. FT-IR reference spectrum of furfural taken from reference [40] (grey) and SEIRA of furfural on Al_2O_3 (blue line), Au (6 wt.%)/Al_2O_3 (black line) and plasmonic TiN nanobars (red line).

Declaration of Competing Interest

The authors declare no competing financial interest.

Acknowledgments

SR, YZ, SK, and AN acknowledge the support of the Czech Science Foundation (GACR) through the award n. 20-17636S and the Ministry of Education, Youth and Sports of the Czech Republic and the Operational Programme Research, Development and Education - European Regional Development Fund, project no. CZ.02.1.01/0.0/0.0/15_003/0000416. EYS and AOG were funded via the ARO grant (contract W911NF-19-20081) and also supported by the Nanoscale and Quantum Phenomena Institute at Ohio University. AOG was also generously supported by the MATH+ Distinguished Visiting Scholarship Award, Berlin, and directly by Zuse Institute, Berlin. SB acknowledges funding by the Deutsche Forschungsgemeinschaft (DFG, German Research Foundation) under Germany´s Excellence Strategy (MATH+, EXC-2046/1, project ID: 390685689). OAB is grateful to US Naval Research Laboratory and Office of Naval Research for financial support.

Appendix A. Supporting Information

Supporting Information contains Methods, materials characterization, theoretical results, photocatalysis and SEIRA data. Supplementary data associated with this article can be found in the online version at doi:

References

[1] M. Kauranen, A. V. Zayats, Nonlinear Plasmonics. *Nat. Photonics* 6 (2012) 737–748. https://doi.org/10.1038/nphoton.2012.244.

[2] H.-L. Wang, E.-M. You, R. Panneerselvam, S.-Y. Ding, Z.-Q. Tian, Advances of Surface-Enhanced Raman and IR Spectroscopies: From Nano/Microstructures to Macro-Optical Design. *Light Sci. Appl.* 10 (2021) 161. https://doi.org/10.1038/s41377-021-00599-2.

[3] L. Mascaretti, A. Schirato, R. Zbořil, Š. Kment, P. Schmuki, A. Alabastri, A. Naldoni, Solar Steam Generation on Scalable Ultrathin Thermoplasmonic TiN Nanocavity Arrays. *Nano Energy* 83 (2021) 105828. https://doi.org/10.1016/j.nanoen.2021.105828.

[4] J. Cunha, T.-L. Guo, G. Della Valle, A. N. Koya, R. Proietti Zaccaria, A. Alabastri, Controlling Light, Heat, and Vibrations in Plasmonics and Phononics. *Adv. Opt. Mater.* 8 (2020) 2001225. https://doi.org/10.1002/adom.202001225.

[5] E. Cortés, L. V. Besteiro, A. Alabastri, A. Baldi, G. Tagliabue, A. Demetriadou, P. Narang, Challenges in Plasmonic Catalysis. *ACS Nano* 14 (2020) 16202–16219. https://doi.org/10.1021/acsnano.0c08773.

[6] L. Mascaretti, A. Naldoni, Hot Electron and Thermal Effects in Plasmonic Photocatalysis. *J. Appl. Phys.* 128 (2020) 041101. https://doi.org/10.1063/5.0013945.

[7] L. Zhou, D. F. Swearer, C. Zhang, H. Robatjazi, H. Zhao, L. Henderson, L. Dong, P. Christopher, E. A. Carter, P. Nordlander, N. J. Halas, Quantifying Hot Carrier and Thermal Contributions in Plasmonic Photocatalysis. *Science* 362 (2018) 69–72. https://doi.org/10.1126/science.aat6967.

[8] R. Kamarudheen, G. J. W. Aalbers, R. F. Hamans, L. P. J. Kamp, A. Baldi, Distinguishing Among All Possible Activation Mechanisms of a Plasmon-Driven Chemical Reaction. *ACS Energy Lett.* 5 (2020) 2605–2613. https://doi.org/10.1021/acsenergylett.0c00989.

[9] A. Naldoni, V. M. Shalaev, M. L. Brongersma, Applying Plasmonics to a Sustainable Future. *Science* 356 (2017) 908–909. https://doi.org/10.1126/science.aan5802

[10] A. Agrawal, S. H. Cho, O. Zandi, S. Ghosh, R. W. Johns, D. J. Milliron, Localized Surface Plasmon Resonance in Semiconductor Nanocrystals. *Chem. Rev.* 118 (2018) 3121–3207. https://doi.org/10.1021/acs.chemrev.7b00613.

[11] W. Li, U. Guler, N. Kinsey, G. V. Naik, A. Boltasseva, J. Guan, V. M. Shalaev, A. V. Kildishev, Refractory Plasmonics with Titanium Nitride: Broadband Metamaterial Absorber. *Adv. Mater.* 26 (2014) 7959–7965. https://doi.org/10.1002/adma.201401874.

[12] A. Naldoni, Z. A. Kudyshev, L. Mascaretti, S. P. Sarmah, S. Rej, J. P. Froning, O. Tomanec, J. E. Yoo, D. Wang, Š. Kment, T. Montini, P. Fornasiero, V. M. Shalaev, P. Schmuki, A. Boltasseva, R. Zbořil, Solar Thermoplasmonic Nanofurnace for High-Temperature Heterogeneous Catalysis. *Nano Lett.* 20 (2020) 3663–3672. https://doi.org/10.1021/acs.nanolett.0c00594.

[13] A. Naldoni, U. Guler, Z. Wang, M. Marelli, F. Malara, X. Meng, L. V. Besteiro, A. O. Govorov, A. V. Kildishev, A. Boltasseva, V. M. Shalaev, Broadband Hot-Electron Collection for Solar Water Splitting with Plasmonic Titanium Nitride. *Adv. Opt. Mater.* 5 (2017) 1601031. https://doi.org/10.1002/adom.201601031.

[14] X. Zhuo, X. Zhu, Q. Li, Z. Yang, J. Wang, Gold Nanobipyramid-Directed Growth of Length-Variable Silver Nanorods with Multipolar Plasmon Resonances. *ACS Nano* 9 (2015) 7523–7535. https://doi.org/10.1021/acsnano.5b02622.

[15] F. Tong, Z. Lou, X. Liang, F. Ma, W. Chen, Z. Wang, Y. Liu, P. Wang, H. Cheng, Y. Dai, Z. Zheng, B. Huang, Plasmon-Induced Dehydrogenation of Formic Acid on Pd-Dotted Ag@Au Hexagonal Nanoplates and Single-Particle Study. *Appl. Catal., B* 277 (2020) 119226. https://doi.org/10.1016/j.apcatb.2020.119226.

[16] I. Kriegel, C. Jiang, J. Rodríguez-Fernández, R. D. Schaller, D. V. Talapin, E. da Como, J. Feldmann, Tuning the Excitonic and Plasmonic Properties of Copper Chalcogenide Nanocrystals. *J. Am. Chem. Soc.* 134 (2012) 1583–1590. https://doi.org/10.1021/ja207798q.

[17] X. Y. Gan, E. L. Keller, C. L. Warkentin, S. E. Crawford, R. R. Frontiera, J. E. Millstone, Plasmon-Enhanced Chemical Conversion Using Copper Selenide Nanoparticles. *Nano Lett.* 19 (2019) 2384–2388. https://doi.org/10.1021/acs.nanolett.8b05088.

[18] J. Cui, Y. Li, L. Liu, L. Chen, J. Xu, J. Ma, G. Fang, E. Zhu, H. Wu, L. Zhao, L. Wang, Y. Huang, Near-Infrared Plasmonic-Enhanced Solar Energy Harvest for Highly Efficient Photocatalytic Reactions. *Nano Lett.* 15 (2015) 6295–6301. https://doi.org/10.1021/acs.nanolett.5b00950.

[19] Y. Liu, Z. Zhang, Y. Fang, B. Liu, J. Huang, F. Miao, Y. Bao, B. Dong, IR-Driven Strong Plasmonic-Coupling on Ag Nanorices/$W_{18}O_{49}$ Nanowires Heterostructures for Photo/Thermal Synergistic Enhancement of H_2 Evolution from Ammonia Borane. *Appl. Catal., B* 252 (2019) 164–173. https://doi.org/10.1016/j.apcatb.2019.04.035.

[20] N. Lu, Z. Zhang, Y. Wang, B. Liu, L. Guo, L. Wang, J. Huang, K. Liu, B. Dong, Direct Evidence of IR-Driven Hot Electron Transfer in Metal-Free Plasmonic $W_{18}O_{49}$/Carbon

Heterostructures for Enhanced Catalytic H_2 Production. *Appl. Catal., B* 233 (2018) 19–25. https://doi.org/10.1016/j.apcatb.2018.03.073.

[21] Z. Zhang, X. Jiang, B. Liu, L. Guo, N. Lu, L. Wang, J. Huang, K. Liu, B. Dong, IR-Driven Ultrafast Transfer of Plasmonic Hot Electrons in Nonmetallic Branched Heterostructures for Enhanced H_2 Generation. *Adv. Mater.* 30 (2018) 1705221. https://doi.org/10.1002/adma.201705221.

[22] T. Paik, M. Cargnello, T. R. Gordon, S. Zhang, H. Yun, J. D. Lee, H. Y. Woo, S. J. Oh, C. R. Kagan, P. Fornasiero, C. B. Murray, Photocatalytic Hydrogen Evolution from Substoichiometric Colloidal WO_{3-x} Nanowires. *ACS Energy Lett.* 3 (2018) 1904–1910. https://doi.org/10.1021/acsenergylett.8b00925.

[23] H. Cheng, T. Kamegawa, K. Mori, H. Yamashita, Surfactant-Free Nonaqueous Synthesis of Plasmonic Molybdenum Oxide Nanosheets with Enhanced Catalytic Activity for Hydrogen Generation from Ammonia Borane under Visible Light. *Angew. Chem. Int. Ed.* 53 (2014) 2910–2914. https://doi.org/10.1002/anie.201309759.

[24] Y. Li, M. Wen, Y. Wang, G. Tian, C. Wang, J. Zhao, Plasmonic Hot Electrons from Oxygen Vacancies for Infrared Light-Driven Catalytic CO_2 Reduction on Bi_2O_{3-x}. *Angew. Chem. Int. Ed.* 60 (2021) 910–916. https://doi.org/10.1002/anie.202010156.

[25] S. Askari, D. Mariotti, J. E. Stehr, J. Benedikt, J. Keraudy, U. Helmersson, Low-Loss and Tunable Localized Mid-Infrared Plasmons in Nanocrystals of Highly Degenerate. *Nano Lett.* 18 (2018) 5681–5687. https://doi.org/10.1021/acs.nanolett.8b02260.

[26] S. Law, V. Podolskiy, D. Wasserman, Towards Nano-Scale Photonics with Micro-Scale Photons: The Opportunities and Challenges of Mid-Infrared Plasmonics. *Nanophotonics* 2 (2013) 103–130. https://doi.org/10.1515/nanoph-2012-0027.

[27] L. Dong, X. Yang, C. Zhang, B. Cerjan, L. Zhou, M. L. Tseng, Y. Zhang, A. Alabastri, P. Nordlander, N. J. Halas, Nanogapped Au Antennas for Ultrasensitive Surface-Enhanced Infrared Absorption Spectroscopy. *Nano Lett.* 17 (2017) 5768–5774. https://doi.org/10.1021/acs.nanolett.7b02736.

[28] S. Bagheri, C. M. Zgrabik, T. Gissibl, A. Tittl, F. Sterl, R. Walter, S. De Zuani, A. Berrier, T. Stauden, G. Richter, E. L. Hu, H. Giessen, Large-Area Fabrication of TiN Nanoantenna Arrays for Refractory Plasmonics in the Mid-Infrared by Femtosecond Direct Laser Writing and Interference Lithography. *Opt. Mater. Express* 5 (2015) 2625. https://doi.org/10.1364/OME.5.002625.

[29] Y. Chen, S. Ji, W. Sun, Y. Lei, Q. Wang, A. Li, W. Chen, G. Zhou, Z. Zhang, Y. Wang, L. Zheng, Q. Zhang, L. Gu, X. Han, D. Wang, Y. Li, Engineering the Atomic Interface

with Single Platinum Atoms for Enhanced Photocatalytic Hydrogen Production. *Angew. Chem. Int. Ed.* 59 (2020) 1295–1301. https://doi.org/10.1002/anie.201912439.

[30] G. Xiang, T. Li, J. Zhuang, X. Wang, Large-Scale Synthesis of Metastable TiO_2(B) Nanosheets with Atomic Thickness and Their Photocatalytic Properties. *Chem. Commun.* 46 (2010) 6801–6803. https://doi.org/10.1039/c0cc02327b.

[31] S. Rej, L. Mascaretti, E. Y. Santiago, O. Tomanec, Š. Kment, Z. Wang, R. Zbořil, P. Fornasiero, A. O. Govorov, A. Naldoni, Determining Plasmonic Hot Electrons and Photothermal Effects during H_2 Evolution with TiN–Pt Nanohybrids. *ACS Catal.* 10 (2020) 5261–5271. https://doi.org/10.1021/acscatal.0c00343.

[32] A. O. Govorov, W. Zhang, T. Skeini, H. Richardson, J. Lee, N. A. Kotov, Gold Nanoparticle Ensembles as Heaters and Actuators: Melting and Collective Plasmon Resonances. *Nanoscale Res. Lett.* 1 (2006) 84−90. https://doi.org/10.1007/s11671-006-9015-7.

[33] H. H. Richardson, M. T. Carlson, P. J. Tandler, P. Hernandez, A. O. Govorov, Experimental and theoretical studies of light-to-heat conversion and collective heating effects in metal nanoparticle solutions, *Nano Lett.* 9 (2009) 1139−1146. https://doi.org/10.1021/nl8036905.

[34] P. Christopher, H. Xin, A. Marimuthu, S. Linic, Singular Characteristics and Unique Chemical Bond Activation Mechanisms of Photocatalytic Reactions on Plasmonic Nanostructures. *Nat. Mater.* 11 (2012) 1044–1050. https://doi.org/10.1038/nmat3454.

[35] K. Li, N. J. Hogan, M. J. Kale, N. J. Halas, P. Nordlander, P. Christopher, Balancing Near-Field Enhancement, Absorption, and Scattering for Effective Antenna–Reactor Plasmonic Photocatalysis. *Nano Lett.* 17 (2017) 3710–3717. https://doi.org/10.1021/acs.nanolett.7b00992.

[36] Y. Kim, J. G. Smith, P. K. Jain, Harvesting Multiple Electron–Hole Pairs Generated through Plasmonic Excitation of Au Nanoparticles. *Nat. Chem.* 10 (2018) 763–769. https://doi.org/10.1038/s41557-018-0054-3.

[37] P. Christopher, H. Xin, S. Linic, Visible-Light-Enhanced Catalytic Oxidation Reactions on Plasmonic Silver Nanostructures. *Nat. Chem.* 3 (2011) 467–472. https://doi.org/10.1038/nchem.1032.

[38] M. Melchionna, P. Fornasiero, Updates on the Roadmap for Photocatalysis. *ACS Catal.* 10 (2020) 5493–5501. https://doi.org/10.1021/acscatal.0c01204.

[39] N. Luo, T. Montini, J. Zhang, P. Fornasiero, E. Fonda, T. Hou, W. Nie, J. Lu, J. Liu, M. Heggen, L. Lin, C. Ma, M. Wang, F. Fan, S. Jin, F. Wang, Visible-Light-Driven Coproduction of Diesel Precursors and Hydrogen from Lignocellulose-Derived Methylfurans. *Nat. Energy* 4 (2019) 575–584. https://doi.org/10.1038/s41560-019-0403-5.

[40] P.J. Linstrom, W.G. Mallard, Eds., NIST Chemistry WebBook, NIST Standard Reference Database Number 69, National Institute of Standards and Technology, Gaithersburg MD, 20899, https://doi.org/10.18434/T4D303, (retrieved December 17, 2021).

Sourav Rej currently working as postdoctoral research fellow in the photoelectrochemistry group at the Regional Centre of Advanced Technologies and Materials, Palacký University, Czech Republic. He received Ph.D. degree (2015) from National Tsing Hua University, Taiwan in shape-controlled synthesis of nanocrystals and their facet dependent catalytic applications under the supervision of Prof. Michael. H. Huang. He then finished next postdoctoral appointment in Institute of Bioengineering & Nanotechnology, A*STAR, Singapore. Now his research interests focus on utilization of plasmonic, semiconductor materials and single atom catalysis for solar energy conversion.

Eva Yazmin Santiago is a PhD candidate at Ohio University, United States. Her research mainly focuses on the computation of optical and electronic properties of nanostructures. She obtained her bachelor's degree in Physics from the National Autonomous University of Mexico (UNAM), where she was awarded the Juan Manuel Lozano Mejía medal. While at Ohio University, she has also been awarded the NQPI Fellowship and the Best Speaker Award at the META Conference in 2022.

Olga A. Baturina is a Research Chemist at the US Naval Research Laboratory. Her area of expertise includes electrochemical energy conversion and storage, electrocatalysis, synthesis of fuels, and photoelectrochemistry. She (co)authored more than 80 paper in peer-reviewed journals and 4 book chapters.

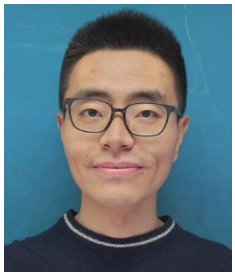

Yu Zhang completed his Ph.D. degree at the Universe of Bologna in 2017. Now, he is a postdoctoral researcher at the Regional Centre of Advanced Technologies and Materials (RCPTM), Palacký University, Olomouc. His research interests focus on the design of electrochemical processes for oxygen reduction reaction and CO_2 reduction reaction.

Sven Burger received a PhD in physics from the University of Hannover, Germany. Currently he heads the Computational Nano Optics research group at Zuse Institute Berlin, Germany. He is further a member of the Berlin Joint Lab for Optical Simulations in Energy Research, of the Mathematics research centre MATH+, and of the board of JCMwave, a spin-off company from Zuse Institute Berlin. His current research fields are in modelling, simulation and optimization related to applications in optics and photonics.

Stepan Kment received his PhD in solid state physics and photoelectrochemistry in 2010 from Czech Technical University in Prague, Czech Republic. He then spent one year as a postdoctoral research fellow at Department of Electrical Engineering, University of Nebrasca – Lincoln, Lincoln, NE, USA. Since 2011 he has been working at Palacky University, Olomouc, Czech Republic as a group leader of Photoelectrochemistry. In addition, He is also working at VSB - Technical University of Ostrava, Czech Republic. His research is focused on development of new materials and nanostructures for PEC water splitting application mainly via advanced plasma deposition methods.

Alexander O. Govorov is a Distinguished Professor of Physics at Ohio University, United States. His research focuses on the theory of optical and electronic properties of nanostructures and bio-assemblies. His theoretical predictions have motivated experiments and have been implemented in many research labs worldwide. Dr. Govorov is the author of more than 340 papers and 2 patents. He is a Fellow of the American Physical Society and the recipient of several international awards including the Bessel Research Award (A. V. Humboldt Foundation), the Walton Visitor Award (Ireland), Zuse-Institute MATH+ Award (Berlin, Germany), etc.

Alberto Naldoni is currently an Associate Professor at University of Turin, Italy. Since 2017 he is also the co-leader of the photoelectrochemistry group at the Regional Centre of Advanced Technologies and Materials of Palacký University Olomouc, Czech Republic. He obtained his Ph.D. in Chemical Sciences from University of Milan (2010) before moving to the Institute of Molecular Sciences and Technologies (ISTM) of the Italian National Research Council in Milan. He spent three years as a visiting faculty at the Birck Nanotechnology Center of Purdue University to investigate alternative plasmonic materials. His group focuses on nanomaterials for plasmonics, photocatalysis, and photoelectrochemistry.